Deep structure of the Porcupine Basin from wide-angle seismic data

Louise Watremez, Manel Prada, Tim Minshull, Brian O 'Reilly, Chen Chen, Tim Reston, Pat Shannon, Gerlind Wagner, Viola Gaw, Dirk Klaeschen, et al.

▶ To cite this version:

Louise Watremez, Manel Prada, Tim Minshull, Brian O 'Reilly, Chen Chen, et al.. Deep structure of the Porcupine Basin from wide-angle seismic data. Geological Society, London, Petroleum Geology Conference series, 2016, pp.1-30. 10.1144/PGC8.26 . hal-01399022

Deep structure of the Porcupine Basin from wide-angle seismic data

Louise Watremez[1*], Manel Prada[2], Tim Minshull[1], Brian O'Reilly[2], Chen Chen[1], Tim Reston[3], Pat Shannon[4], Gerlind Wagner[5], Viola Gaw[5], Dirk Klaeschen[5], Rose Edwards[6] and Sergei Lebedev[2]

[1]*Ocean and Earth Science, National Oceanography Centre Southampton, University of Southampton, Southampton, UK*

[2]*Geophysics Section, Dublin Institute for Advanced Studies, Dublin, Ireland*

[3]*School of Geography, Earth and Environmental Sciences, University of Birmingham, Birmingham, UK*

[4]*School of Earth Sciences, University College Dublin, Dublin, Ireland*

[5]*Geomar Helmholtz Centre for Ocean Research, Kiel, Germany*

[6]*National Oceanography Centre, Southampton, UK*

[*]*Corresponding author (e-mail: L.D.Watremez@soton.ac.uk)*

Abbreviated title: Deep structure of Porcupine Basin

ABSTRACT

The Porcupine Basin, part of the frontier petroleum exploration province west of Ireland, has an extended history that commenced prior to the opening of the North Atlantic Ocean. Lithospheric stretching factors have previously been estimated to increase from <2 in the north to >6 in the south of the basin. Thus, it is an ideal location to study the processes leading to hyperextension on continental margins. The Porcupine Median Ridge (PMR) is located in the south of the basin and has been alternatively interpreted as a volcanic feature, a serpentinite mud diapir, or a tilted block of continental crust. Each of these interpretations has different implications for the thermal history of the basin. We present results from travel-time tomographic modelling of two ~300-km-long wide-angle seismic profiles across the northern and southern parts of the basin. Our results show: (1) the geometry of the crust, with maximum crustal stretching factors up to 6 and 10 along the northern and southern profiles, respectively; (2) asymmetry of the basin structures, suggesting some simple shear

during the extension; (3) low velocities beneath the Moho that could represent either partially serpentinised mantle or mafic under-plating; and (4) a possible igneous composition of the PMR.

Keywords: Porcupine Basin, rifting, crustal thinning, seismic refraction

Rifted continental margins are important locations for oil and gas provinces, highlighted by the recent discoveries along the Atlantic conjugate margins and elsewhere (Mann *et al.* 2003; Levell *et al.* 2010). The evaluation of the structure of sedimentary basins in such rifted margins, and the processes involved in their formation, are key to understanding the thermo-mechanical evolution of rifted margin systems. This understanding is essential in constraining, for example, regional stratigraphic development and time-temperature history of petroleum source rocks (e.g. White *et al.* 2003; Hantschel & Kauerauf 2009; Wangen 2010).

The Porcupine Basin, located west of Ireland, is an ideal natural laboratory to investigate these processes as the degree of crustal thinning varies dramatically from north to south (e.g. Tate *et al.* 1993; Readman *et al.* 2005). Different parts of the basin may reflect and preserve evidence of different stages of continental rifting. The basin is underlain by thin to ultra-thin continental crust (O'Reilly *et al.* 2006) and is therefore an excellent location in which to investigate the processes associated with hyperextension (e.g. mantle serpentinisation; Reston *et al.* 2001).

The basin is lightly explored, with only 31 exploration and appraisal wells. There have been two oil and one gas condensate discoveries to date in the north of the basin (Naylor & Shannon 2011) and a number of other key wells, such as the recent Dunquin North 44/23-1 well, that confirmed the components of a working petroleum system in the centre of the basin (Wrigley *et al.* 2014). The recent increase in exploration interest, reflected in new Licensing Option awards, suggests that it will remain an active frontier exploration province in the coming years. However, unlocking the petroleum potential will require an improved understanding of basin structure and development (Wrigley *et al.* 2014).

In this paper, we use wide-angle seismic data along two West-East lines that cross the Porcupine Basin axis, from the Porcupine Bank to the Irish Continental Shelf at 52.2°N and 51.4-51.5°N (Fig. 1), to provide an analysis of the crustal and uppermost mantle seismic velocities across the basin and briefly consider implications for its formation.

GEOLOGICAL BACKGROUND

The sedimentary record of the Porcupine Basin reveals a complex geodynamic and/or thermal history involving several episodes of rifting and subsidence that span from late Palaeozoic to late Mesozoic times, with the major rift phase occurring in Late Jurassic – Early Cretaceous times (Shannon 1991; Tate *et al.* 1993; Johnston *et al.* 2001; Naylor & Shannon 2011).

Based on subsidence analysis from available seismic reflection and well data, and using a simple Airy isostatic approach, Tate *et al.* (1993) estimated that lithospheric stretching factors increase from less than 2 in the north to more than 6 in the south of the Porcupine Basin (Fig. 1). Crustal thicknesses in Porcupine Basin have been estimated by 3D gravity modelling, with minimum thicknesses in the centre of the basin as low as 5 km (Welford *et al.* 2012). Recent results from wide-angle seismic data (O'Reilly *et al.*; 2006) suggest that the crust is even thinner in places and may be absent in the central part of the basin, over the Porcupine Arch (Fig. 1c). This observation may imply that the basin has experienced a more complex stretching history resulting in greater thinning, at least locally in the centre of the basin, than estimated by Tate *et al.* (1993).

Tate *et al.* (1993) also described a ridge feature, the Porcupine Median Ridge (hereafter, the PMR), in the middle of the southernmost part of the basin (Fig. 1). This feature was described further by Naylor *et al.* (1999, 2002). During the last three decades, this ridge has been successively interpreted as (1) a volcanic structure (e.g. Tate & Dobson 1988; White *et al.* 1992; Calvès *et al.* 2012); (2) a serpentinite mud diapir (Reston *et al.*, 2001, 2004); or (3) a block of continental crust (e.g., O'Sullivan *et al*. 2010; Hardy *et al.* 2010). Its nature is still debated.

Another striking feature is observed in the free-air gravity data: the Porcupine Arch (Fig. 1c), first described and named by Naylor *et al.* (2002). This feature appears as a gravity high and has been interpreted as the result of a very thin crust overlying partially serpentinised uppermost mantle

(Readman *et al.* 2005; O'Reilly *et al.* 2006). In contrast, the PMR is not evident in the gravity data (Fig. 1c). Readman *et al.* (2005) attributed the rapid variation of the gravity anomaly at the south of the Porcupine Arch to the presence of a major change of crustal thickness resulting from a transfer zone, involving different tectonic regimes in the northern and southern Porcupine Basin.

DATA AND METHOD

The data acquisition and seismic phases

The data used in this study were acquired during an offshore/onshore wide-angle-seismic experiment that was completed by GEOMAR and DIAS in May 2004.

The northern profile

The northern profile is a 270 km shot line running across the Porcupine Basin, from West to East, at 52.2°N. Here, 2258 shots were recorded by 22 sea-bottom instruments (Fig. 1c): ten ocean bottom hydrophones (OBH) and twelve ocean bottom seismometers (OBS). Data are of generally good quality (Figs. 2a and 2c), allowing the identification of seismic arrivals to up to 110 km distance between the source and the receiver. A thorough study of the seismograms allowed for the identification of thirteen seismic phases: the arrivals of refractions turning in seven different layers and wide-angle reflections at the corresponding six geological interfaces. The four shallowest layers are observed on most instruments of the central part of the basin. They correspond to sedimentary layers and show apparent velocities of 1.5-1.6 km/s, 2 km/s, 2.75 km/s and 3.75 km/s, from top to bottom. The refracted arrivals of the three deeper layers are observed at further offsets, with apparent velocities of 5-5.5 km/s, 6-6.5 km/s and 7.5-8 km/s, which are typical for two crustal layers and the upper mantle, respectively.

The southern profile

A total of 31 ocean-bottom instruments were deployed along the 307-km-long southern line. First, ten OBH and fifteen OBS were deployed every ~8 km along a 2D line and recorded 2523 shots: instruments 1 to 25 (Fig. 1c). However, OBH 05 and 24 failed to record useable data and a second seismic survey taking place in the study area at the same time made the easternmost part of the line very noisy. For this reason, part of the line was re-shot later. Then, six ocean-bottom instruments were deployed and 702 shots were recorded by instruments 90 to 95 (Fig. 1c). The location of the instruments was chosen to increase the data density above the Porcupine Median Ridge, reducing the instrument spacing along this profile down to 4 km in the central part of the line. Apart from the easternmost part of the first shot line, the data are of very good quality (Figs. 2e and 2g), showing good arrivals to source-receiver distances of 80-120 km on most instruments. The seismograms allow the identification of eleven seismic phases: six refractions and five wide-angle reflections. Three sedimentary layers were identified, with apparent velocities of 2.5 km/s, 3.25 km/s and 5-5.25 km/s, from top to bottom. The third sedimentary refracted phase corresponds to arrivals of rays turning in the lowermost sediments and the PMR. As for the northern profile, arrivals from the three deeper layers corresponded to two crustal layers and the upper mantle. These arrivals had apparent velocities of 5.5-6 km/s, 6.5-7 km/s and 7-8 km/s, respectively.

Data processing and picking

The phases identified on each seismogram were picked manually. In total, 31,676 and 62,977 arrivals were picked along the northern and southern profiles, respectively (Tables 1 and 2).

Data were picked on unprocessed seismograms first, using both hydrophone and vertical geophone, where available. Further arrivals were picked using deconvolved and filtered seismograms. These later picks were done with care to avoid introducing a time shift in the picking. Deconvolution was done in 2 steps: (1) spiking deconvolution, and (2) predictive deconvolution, with a gap length of 0.386 s. Then, a band-pass filter was applied, with corner frequencies of 1-5-15-25 Hz. Processed data were also used for display (Fig. 2). This processing significantly improved the signal-to-noise ratio and allowed for the retrieval of signal at far offsets, up to source-receiver distances of 100-120 km. Some instruments show a high velocity set of arrivals at source-receiver distances of 5-20 km (e.g. black arrows on Fig. 2h). These arrivals correspond to a 5-5.25 km/s layer in the sediments that is probably thin (up to a few hundred meters) and would be poorly resolved by travel-time tomography. Thus, we ignored these arrivals in this study.

Picking uncertainties were set using the signal to noise ratio of the data trace 250 ms before and after the picked arrival for each arrival time, following Zelt & Forsyth's (1994) empirical relationship, and an offset dependent relationship for offsets < 40 km. Thus, picking uncertainties vary from 20 to 125 ms.

Modelling strategy

Picks from both lines were modelled using the Tomo2D code (Korenaga *et al.* 2000). This tomography method solves the forward problem by first obtaining the residual travel times by means of ray-tracing and then solving a linearised inverse problem to reduce the residuals. Since the initial model is always far from the solution, the linearised inverse problem has to be solved iteratively. To prevent excessive model perturbation, the method includes some regularisation represented by velocity and depth smoothing (parameterised by correlation lengths) and damping constraints to stabilise the iterative inversion.

The picked phases were inverted following a layer stripping strategy (Sallarès et al. 2011) to allow for imaging wide-angle reflections together with the corresponding refracted phases. Thus, we proceeded by building the model layer by layer, resolving at each step the velocity and depth structure of a layer, from top to bottom.

For each step, starting velocity models were built using the apparent velocities observed on the seismograms together with the velocities and reflector depth from the previous layer. Moho depth beneath the Irish Continental Shelf, southwest of Ireland, was constrained using the results of an onshore refraction study (O'Reilly *et al.* 2010).

The velocity models of the Northern and Southern profiles were built in seven and six steps, respectively (Figs. 3a and 3b). At each step, the resulting models reproduce well the picks within their uncertainties (χ^2 values lower than 1, Tables 1 and 2). An indication of the density of the ray coverage in the final models is provided by the derivative weight sum (DWS, Figs. 3c and 3d). The DWS gives an indication of which areas of the models are better resolved. The central and shallow areas of the models have the densest ray coverage. Thus, this is where we can expect the best resolution and reliability of results.

VELOCITY MODELS

The velocity models show the geometry of the sedimentary basin, the thinning of the crust and the velocity structure in the uppermost mantle (Fig. 3a and 3b).

Northern line

The tomography model of the northern profile shows the P-wave velocity structure in the sediments, crust and upper mantle together with the geometry of the six reflectors: four in the sediments, one in the basement and the Moho (Fig. 3a).

The velocity structure from the seafloor down to the deepest sedimentary reflection shows velocities ranging from 1.6 to ~3.5 km/s (Fig. 4a). These velocities are characteristic of post-rift sediments (Cenozoic to Cretaceous) according to previous refraction studies in the area (O'Reilly *et al.* 2006). Also, the lateral continuity of these layers indicates no significant evidence of disruption or deformation that could be attributed to the effects of active fault-controlled rifting. Below these, no wide-angle reflectivity from the syn-rift and pre-rift sections is identified on the record sections, and thus, no interface bounding these layers is retrieved in this model. However, velocities of 4-5 km/s might correspond to isolated syn-rift packages rotated by normal faults, e.g. at 90 km model distance and 7 km depth (Fig. 3a). Below these packages, an intra-basement reflector is defined across the basin, showing a velocity contrast from 5 to 5.5 km/s in some regions. The velocities observed in this layer might represent either pre-rift sediments or fractured crystalline crust. Below this intra-basement reflector, seismic velocities increase downwards from 5.5-6 to 6.8-6.9 km/s at the Moho discontinuity (Fig. 4a), which shows major asymmetry across the basin. The lowermost basement shows velocities up to 6.8-6.9 km/s where the crust is thick and up to 6.5 km/s in the central part of the basin where the crust is highly thinned (km 100-130, see Fig. 4a). The model shows a strong velocity contrast, from 6.5-7 to more than 7.5 km/s, at the Moho discontinuity. Seismic velocities range from 7.5 to ~8.1 km/s in the uppermost mantle. Interestingly, we observe velocities as low as 7.4 km/s at model distances of 90 and 115 km in the uppermost mantle (Fig. 4a), coinciding with the progressive eastward thinning of the crust.

In summary, the northern profile features: (1) an 8-9 km thick post-rift sedimentary sequence, (2) an asymmetric crustal structure, and (3) crustal thinning from 30 km near the Irish coastline to less than 5 km in the central part of the basin (km 120), using a velocity contour of 5 km/s for the top of the crystalline basement and the Moho reflection for the base of the crust.

Southern line

The tomography model for the southern profile shows the velocity structure in the sediments, crust and upper mantle together with the geometry of the five reflectors (Fig. 3b). The first two sedimentary layers show velocities of 1.65 to 3.0 km/s and 3.0 to 3.5 km/s, respectively (Fig. 4b). The third layer corresponds to the deepest sedimentary layer together with the PMR. This third layer shows higher velocities, reaching 6 km/s in the middle of the basin, at model distances of 155 to 185 km, corresponding to the location of the PMR (Fig. 4b). These velocities are consistent with a volcanic origin but do not exclude other interpretations. On the eastern side of the PMR, velocities are typical for compacted sediments. There is little velocity contrast between the PMR and surrounding sediments, and reflections from the top of the PMR are few. Thus, for our modelling, we decided to model the ridge and adjacent sub-basins as a single layer. We modelled high velocities on the western side of the ridge, with values of 5 to 5.2 km/s at model distances of 140 to 160 km and depths of 6-7 km. These velocities would also be consistent with a volcanic origin. These high velocities are observed near the top of the PMR. Beneath this layer, we modelled the basement as two layers. The upper basement generally shows velocities of 5-5.5 to 6 km/s. The velocities of 5-5.5 km/s might correspond to compacted pre-rift sediments or highly fractured crystalline basement. The lower basement shows velocities of 6-7 km/s (Fig. 4b). The velocity contrast between upper and lower basement is most obvious in the centre of the basin, at model distances of 120 to 200 km. Uppermost mantle velocities range from 7 km/s beneath the western part of the basin to 7.5 km/s in the centre, at a model distance of 160 km, just beneath the PMR, and decrease slightly to the East, with a velocity of 7.3 km/s just beneath the Moho (Fig. 4b). However, the velocities of 7 km/s beneath the western part of the basin are poorly resolved as this area is covered by few rays, all propagating eastward (Fig. 3d).

Thus, the southern profile features: (1) a 7 km thick post-rift sedimentary sequence with velocities up to 4-4.5 km/s, (2) a high velocity area in the central part of the basin, corresponding to the PMR, and an adjacent high velocity layer, showing seismic velocities consistent with a volcanic origin, (3) asymmetric crustal thinning compatible with a component of simple shear along a detachment surface during the extension, (4) a wide zone of highly thinned crust, where the crust is 6 km thick or less over a 90 km wide area, and could be as thin as 3 km at km 150, and (5) an uppermost mantle with velocities of 7.3 to 7.5 km/s just below the Moho.

COMPARISON WITH BOREHOLE AND REFLECTION DATA

Comparison of modelled velocities with well log data

Comparison of borehole seismic velocity measurements with our models can aid interpretation, and is also a way to validate our model. Sonic velocities compare well with the two models, generally differing by less than 100-200 m/s (Fig. 5). Velocities from wide-angle data show smoother variations than the well data, due to the method: seismic travel-times give an average of the velocities in the subsurface, with lower resolution than well-log data. Note that tomography models produced by the layer-stripping method allow changes in the velocity gradient at interfaces but not abrupt velocity jumps.

Well 35/21-1, which terminated in Eocene strata, is located 5.4 km north of the northern line near a model distance of 114.7 km (Fig. 5a). Comparison of the velocity-depth profile of the well with our tomography model at the projected position of the well along the northern profile shows a good correlation of the overall velocities down to the bottom of the well.

Well 43/13-1, which terminated in Upper-Jurassic strata, is located approximately 7 km north of the southern line near a model distance of 110.5 km (Fig. 5b). The well data and tomography results along the southern line also show a very good correlation of the velocities at depth.

The velocity differences observed between the well log data and the velocity models probably arise because the wells are not located exactly on the velocity profiles and sediment velocities can vary laterally by 100-500 m/s (Fig. 4b).

Comparison of the models with coincident seismic reflection profiles

Combining the velocity models with coincident seismic reflection data allows a comparison between the two images, thereby helping to improve interpretation of the seismic reflection data at depth (Figs. 6 and 7). A Kirchhoff pre-stack depth migration was applied to the seismic reflection data, using velocities from residual move-out and depth focusing analysis in a top down approach. The image output from this method is sharper than the image output using velocities from wide-angle tomography. The RMS differences between velocities from the wide-angle data and velocities used for pre-stack depth migration in the basin area are 0.022 and 0.026 km/s for the northern and southern lines, respectively. There is a remarkable correspondence between the independently-derived velocity models and the coincident seismic reflection profiles.

Northern line

The seismic reflection profile Wire 2 (Croker & Klemperer 1989) is coincident with the northern profile. We compared the velocity structure of the basin with the tectonic structure observed in a pre-stack depth migration of Wire 2 (Fig. 6). Figure 6c shows that the post-rift sedimentary cover has velocities ranging from 1.6 to ~4.0-4.5 km/s. Below this sedimentary package, velocities between 4.5 and 5 km/s overlie rotated syn-tectonic sediments, while velocities between 5 and 6.9 km/s are mainly representative of the crystalline basement, though velocities between 5 and 5.5 km/s might also represent pre-rift sediments. The base of the half-graben structure observed in the middle of the basin (i.e. 120-125 km model distance and 8 km depth, Fig. 6b) is well defined by seismic velocities of 5 km/s that coincide with the crystalline basement. The top of the mantle from the seismic velocity model (Fig. 6c) coincides with high amplitude reflections at 14 km depth and CDP 5700-6500 on profile Wire 2 (Fig. 6b). Thus, these reflections observed on Wire 2 might also correspond to the crust-mantle boundary.

Southern line

The superposition of the velocity model of the southern line with the coincident SPB97-115 seismic reflection profile (Reston *et al.* 2001, 2004) allows us to compare the velocities with the reflectivity (Fig. 7). Velocities from 1.6 to ~5 km/s follow the sedimentary structures. In particular, velocities between 4 and 5 km/s highlight typical syn-rift deposits, i.e. tilted-blocks like those observed along the northern line, at models distances of 105-125 km (Fig. 7c). The PMR, located between CDP 4500 and 6500 at 5 to 9 km depth (Fig 7b), shows velocities from 4.7 km/s at its top to 6 km/s at its base, which are higher than the surrounding sediments. Also, a set of reflectors with higher amplitude than the sediments above and below, is observed in the western part of the basin, at CDP 3000 to 5000, at depths of 5.5 to 7 km (Fig. 7a). These reflectors are coincident with a high velocity layer in the sedimentary sequence, with velocities of 5-5.25 km/s. Also, velocities in the eastern part of the basin, east of the PMR, are generally lower than those in the western part of the basin. The SPB97-115 profile shows some deep reflectivity at approximately 14 km depth, CDP 5500-7000 (Fig. 7b). This reflectivity is coincident with the top of the mantle of the velocity model at km 175-190, where seismic velocities jump from ~6.5 to 7.3 km/s (Fig. 7c). Thus, this deep reflectivity corresponds to the Moho discontinuity.

DISCUSSION

The highly stretched region of Porcupine Basin widens slightly towards the south, from approximately 100 km along the northern profile to 115 km along the southern profile. The width of the region of highly stretched crust, with crustal thicknesses < 6 km, is about 90 km along the southern profile and less than 30 km along the northern profile. These two observations show the extent to which the basin is more stretched in the south than in the north (Figs. 3a and 3b). Also, the crustal structures across both lines are asymmetric, including, in particular, the morphology of the Moho discontinuity. Such asymmetry is compatible with a model in which some of the crustal deformation has been accommodated by simple shear along a crustal discontinuity during rifting. Reston *et al.* (2001) proposed that the rifting in Porcupine Basin changed from a symmetric to an asymmetric mode as upper mantle serpentinisation began as a result of the embrittlement of the crust. Such asymmetry is shown also by numerical models (e.g. Brune et al. 2014; Huismans & Beaumont 2014) and conceptual models built from geological observations in the Alps and West Iberia (e.g. Manatschal 2004).

We calculated maximum stretching factors as the ratio between the assumed pre-rift crustal thickness (30 km; Lowe & Jacob 1989; O'Reilly *et al.* 2010) and the minimum thicknesses of the crystalline basement, 5 and 3 km along the northern and southern lines, respectively. Thus, the maximum crustal stretching factors increase from 6 along the northern line to 10 along the southern line. Greater crustal thicknesses, up to 34 km, have been estimated from a receiver function study beneath southern Ireland (Licciardi *et al.* 2014), so stretching factors may reach even higher values. These values are much greater than the lithospheric stretching factors previously estimated from subsidence (Fig. 1; Tate *et al.* 1993). The maximum lithospheric stretching factors inferred by Tate *et al.* (1993) are only ~2.5 along the northern profile and 5 along the southern profile, which is half or less of the crustal stretching factors obtained in this study. The lithospheric stretching factors were estimated by a subsidence analysis that assumed pure shear extension, made a variety of simplistic assumptions, and used a limited amount of older seismic reflection and well data.

The high crustal stretching factors, 6 and 10, imply that the crust became entirely brittle during the rifting, allowing crustal-scale faults to reach the mantle and the sea water to percolate through these faults and serpentinise the uppermost mantle (O'Reilly *et al.* 1996; Pérez-Gussinyé & Reston 2001). This process is compatible with the low velocities observed in the uppermost mantle, which are 7.4-7.8 km/s along the northern line and only 7.3-7.5 km/s along the southern line. Thus, the mantle velocities decrease significantly from north to south. The observed mantle velocities can be explained by 8 to 20 % serpentinisation along the northern line and approximately 20 % along the southern line (Carlson & Miller 2003). Such velocities are also compatible with the presence of mafic intrusions in the uppermost mantle (e.g. Funck *et al.* 2008). The difference between crustal and inferred lithospheric stretching factors may be attributed to a combination of (1) bias in the lithospheric stretching estimates due to the simplifying assumptions, (2) mantle serpentinisation (O'Reilly *et al.* 1996) beneath the thin crust and/or addition of material at the base of the crust, (3) real differences in stretching factors between the crust and mantle lithosphere, and (4) dynamic topography resulting from the Iceland plume activity (Hartley *et al.* 2011).

Along the southern profile, a basement high corresponds to the PMR, where velocities range from 4.7 to 6 km/s. Similar velocities are observed west of the PMR, overlying high reflectivity in the sedimentary succession (Fig. 7). The seismic velocity of both the PMR and the intra-sedimentary layer is consistent with that of volcanic rocks (e.g. Christensen 1982; Eldholm & Grue 1994). Thus, using both refraction and reflection seismic imaging, we interpret the PMR as a volcanic feature. The velocities in the PMR are slower than might be expected for a serpentinite diapir, reaching values as low as 4.7 km/s. Velocities are also lower than those expected for continental crustal rocks and, based on this observation and the morphology of the ridge, we do not favour the tilted-block hypothesis. At this stage we cannot exclude the serpentinite diapir and tilted-block hypotheses: serpentinite could be mixed with sediments and a tilted crustal block could be highly fractured, also decreasing the velocities. Nevertheless, the geometry and seismic velocities of the PMR favour a volcanic structure. High seismic velocities similar to the PMR velocities and a velocity inversion in the underlying sediments also favour an igneous nature (e.g. intrusive sills or volcanic flows) of the highly reflective intra-sedimentary layer. If these volcanics were related to the PMR, their presence would imply that the PMR had at least two main phases of activity: (1) a first phase during which the volcanic ridge formed, sitting near the base of the post-rift sediments, and (2) a more recent phase, with volcanic flows or sills emplaced during the post-rift sedimentation of the basin. Similar poly-phase magmatic activity has been observed in volcanic islands such as the Canary Islands (e.g. Ancochea *et al.* 2006).

Although a detailed analysis of the thermal evolution of the basin is beyond the scope of the present study, it is worth noting that our results have implications for the amount and timing of heat affecting the sediments, and thus the thermal maturity of Mesozoic source rocks. For example, Naeth *et al.* (2005) used the lithospheric stretching factors (Fig. 1; Tate *et al.* 1993) to estimate the thermal history of the basin, but assumed uniform stretching based upon McKenzie's (1978) model. Our inferred crustal stretching factors are larger than the lithospheric stretching factors inferred by Tate *et al.* (1993). New thermal models are needed to estimate the influence of higher stretching factors on the heat-flow. In addition to the amount and nature of stretching and extensional strain rates, the presence of volcanism of various ages and of serpentinised upper mantle in this area provide additional components to the complex thermal history as well as the tectono-sedimentary evolution of the basin.

CONCLUSIONS

In this study, we determined the crustal and upper mantle structure across Porcupine Basin, from the Porcupine Bank to the Irish shelf, along two east-west profiles, 90 km apart from each other. We conclude that:

- The large-scale crustal structure is highly asymmetric, which is compatible with a component of simple shear during crustal stretching. Crustal thinning increases from north to south in the basin. The continental crust is highly stretched along the whole basin, with maximum crustal stretching factors increasing toward the south, from 6 to 10 between the two profiles. Also, the highly thinned crust occurs across a wider area in the south (90 km) than in the north (< 30 km).
- The PMR shows seismic velocities that are consistent with volcanics but do not exclude other interpretations. The PMR is located just east of a high-velocity / highly reflective layer in the sediment column, which we interpret as of igneous origin. The relationship between this feature and the PMR is unclear.
- Seismic velocities in the upper mantle are lower than those of typical unaltered peridotites, indicating the presence of either partially serpentinised mantle (10-20%, degrees of serpentinisation increasing toward the south) or mafic intrusions beneath the base of the crust, in particular in the southern part of the basin.

ACKNOWLEDGMENTS

This project is funded by the Irish Shelf Petroleum Studies Group (ISPSG) of the Irish Petroleum Infrastructure Programme Group 4. The ISPSG comprises: Atlantic Petroleum (Ireland) Ltd, Cairn Energy Plc, Chrysaor E&P Ireland Ltd, Chevron North Sea Limited, ENI Ireland BV, Europa Oil & Gas (Holdings) plc, ExxonMobil E&P Ireland (Offshore) Ltd., Kosmos Energy LLC, Maersk Oil North Sea UK Ltd, Petroleum Affairs Division of the Department of Communications, Energy and Natural Resources, Providence Resources plc, Repsol Exploración SA, San Leon Energy Plc, Serica Energy Plc, Shell E&P Ireland Ltd, Sosina Exploration Ltd, Statoil (UK) Ltd, Tullow Oil Plc and Woodside Energy (Ireland) Pty Ltd. Gravity, seismic and well data were provided by the Petroleum

Affairs Division of the Department of Communications, Energy & Natural Resources, Ireland. Seismic reflection data along profile SPB97-115 were supplied by Fugro-Geoteam through Conoco-Phillips. Profile Wire2 was acquired during the BIRPS WIRE project, which was funded by the Natural Environment Research Council (UK), the Department of Energy (Ireland) and Western Geophysical. We thank K. Welford and an anonymous reviewer for their constructive comments and suggestions. GMT was used to prepare all the figures (Wessel & Smith 1998) and was combined with Seismic-Unix (Stockwell 1999) for Figures 2, 6 and 7. Minshull was supported by a Wolfson Research Merit award.

REFERENCES

Ancochea, E., Hernán, F., Huertas, M. J., Brändle, J. L. & Herrera, R. 2006. A new chronostratigraphical and evolutionary model for La Gomera: implications for the overall evolution of the Canarian Archipelago. *Journal of Volcanology and Geothermal Research*, **157**(4), 271-293, doi:10.1016/j.jvolgeores.2006.04.001.

Brune, S., Heine, C., Pérez-Gussinyé, M. and Sobolev, S.V. 2014. Rift migration explains continental margin asymmetry and crustal hyper-extension. *Nature Communications*, **5**, doi:10.1038/ncomms5014

Calvès, G., Torvela, T., Huuse, M. & Dinkleman, M. G. 2012. New evidence for the origin of the Porcupine Median Volcanic Ridge: Early Cretaceous volcanism in the Porcupine Basin, Atlantic margin of Ireland. *Geochemistry, Geophysics, Geosystems*, **13**(6), doi:10.1029/2011GC003852.

Carlson, R. L. & Miller, D. J. 2003. Mantle wedge water contents estimated from seismic velocities in partially serpentinized peridotites. *Geophysical Research Letters*, **30**(5), doi:10.1029/2002GL016600.

Christensen, N. I. 1982. Seismic velocities, In: *Handbook of physical properties of rocks*, **2**, 1-228.

Croker, P. F. & Klemperer, S. L. 1989. Structure and Stratigraphy of the Porcupine Basin: Relationships to Deep Crustal Structure and the Opening of the North Atlantic, in *Extensional*

Tectonics and Stratigraphy of the North Atlantic Margins, eds Tankard A.J., Balkwill H.R., *American Association of Petroleum Geologists*, Tulsa, **46**, 445-159.

Eldholm, O. & Grue, K. 1994. North Atlantic volcanic margins: Dimensions and production rates, *Journal of Geophysical Research*, **99**(B2), 2955-2968, doi:10.1029/93JB02879.

Funck, T., Andersen, M. S., Keser Neish, J. & Dahl-Jensen, T. 2008. A refraction seismic transect from the Faroe Islands to the Hatton-Rockall Basin. *Journal of Geophysical Research - Solid Earth*, **113**(B12), doi:10.1029/2008JB005675.

Hantschel, T. and Kauerauf, A.I. 2009. *Fundamentals of basin and petroleum systems modeling*. Springer Science & Business Media.

Hardy, R.J.J., Querendez, E., Biancotto, F., Jones, S.M., O'Sullivan, J. & White, N. 2010. New methods of improving seismic data to aid understanding of passive margin evolution: a series of case histories from offshore west of Ireland. In *Geological Society, London, Petroleum Geology Conference series*, **7**, 1005-1012, doi:10.1144/0071005.

Hartley, R.A., Roberts, G.G., White, N. and Richardson, C. 2011. Transient convective uplift of an ancient buried landscape. *Nature Geoscience*, **4**(8), 562-565, doi:10.1038/ngeo1191.

Huismans, R.S. and Beaumont, C. 2014. Rifted continental margins: the case for depth-dependent extension. *Earth and Planetary Science Letters*, **407**, 148-162, doi:10.1016/j.epsl.2014.09.032.

Johnston, S., Doré, A. G. & Spencer, A. M. 2001. The Mesozoic evolution of the southern North Atlantic region and its relationship to basin development in the south Porcupine Basin, offshore Ireland. *Geological Society, London, Special Publications*, **188**(1), 237-263, doi:10.1144/GSL.SP.2001.188.01.14.

Korenaga, J., Holbrook, W. S., Kent, G. M., Kelemen, P. B., Detrick, R. S., Larsen, H. C., Hopper, J. R. & Dahl-Jensen, T. 2000. Crustal structure of the southeast Greenland margin from joint refraction and reflection seismic tomography. *Journal of Geophysical Research - Solid Earth*, **105**, 21591-21614, doi:10.1029/2000JB900188.

Levell, B., Argent, J., Doré, A. G., & Fraser, S. 2010. Passive margins: overview. In *Geological Society, London, Petroleum Geology Conference series* **7**. Geological Society of London, 823-830.

Licciardi, A., Agostinetti, N. P., Lebedev, S., Schaeffer, A. J., Readman, P.W. & Horan, C. 2014. Moho depth and Vp/Vs in Ireland from teleseismic receiver functions analysis. *Geophyical Journal International*, **199**, 561-579, doi:10.1093/gji/ggu277.

Lowe, C. & Jacob, A.W.B. 1989. A north–south seismic profile across the Caledonian suture zone in Ireland. *Tectonophysics*, **168**(4), 297-318, doi:10.1016/0040-1951(89)90224-2.

Manatschal, G. 2004. New models for evolution of magma-poor rifted margins based on a review of data and concepts from West Iberia and the Alps. *International Journal of Earth Sciences*, **93**(3), 432-466, doi:10.1007/s00531-004-0394-7.

Mann, P., Gahagan, L., & Gordon, M. B. 2003. Tectonic setting of the world's giant oil and gas fields. In *M. T. Halbouty, ed., Giant oil and gas fields of the decade 1990–1999*, AAPG Memoir **78**, 15-105.

McKenzie, D.P. 1978. Some remarks on the development of sedimentary basins. *Earth & Planetary Science Letters*, **40**, 25-32, doi:10.1016/0012-821X(78)90071-7.

Naylor, D. & Shannon, P.M. 2011. *Petroleum Geology of Ireland.* Dunedin Academic Press, Edinburgh, Scotland. 262 pages.

Naylor, D., Shannon, P. & Murphy, N. 1999. *Irish Rockall region – a standard structural nomenclature system.* Petroleum Affairs Division. Special Publication 1/99. 42 pages and 2 Enclosures.

Naylor, D., Shannon, P. & Murphy, N. 2002. *Porcupine-Goban region – a standard structural nomenclature system.* Petroleum Affairs Division. Special Publication 1/02. 65 pages and 2 Enclosures.

Naeth, J., Di Primio, R., Horsfield, B., Schaefer, R. G., Shannon, P. M., Bailey, W. R., & Henriet, J. P. 2005. Hydrocarbon seepage and carbonate mound formation: a basin modelling study from the Porcupine Basin (offshore Ireland). *Journal of Petroleum Geology*, **28**(2), 147-166, doi:10.1111/j.1747-5457.2005.tb00077.x.

O'Reilly, B.M., Hauser, F., Jacob, A.W.B. & Shannon, P.M. 1996. The lithosphere below the Rockall Trough: wide-angle seismic evidence for extensive serpentinisation. *Tectonophysics*, **255**, 1-23, doi:10.1016/0040-1951(95)00149-2.

O’Reilly, B. M., Hauser, F., Ravaut, C., Shannon, P. M. & Readman, P. W. 2006. Crustal thinning, mantle exhumation and serpentinization in the Porcupine Basin, offshore Ireland: evidence from wide-angle seismic data. *Journal of the Geological Society, London*, **163**, 775-787, doi:10.1144/0016-76492005-079.

O'Reilly, B. M., Hauser, F. & Readman, P. W. 2010. The fine-scale structure of upper continental lithosphere from seismic waveform methods: insights into Phanerozoic crustal formation processes. *Geophysical Journal International*, **180**(1), 101-124, doi:10.1111/j.1365-246X.2009.04420.x.

O'Sullivan, J. M., Jones, S. M. & Hardy, R. J. 2010. Comparative analysis of the Porcupine Median Volcanic Ridge with modern day Pacific Ocean seamounts–further evidence of an amagmatic Mesozoic basin history for the South Porcupine Basin, offshore Ireland. *Conjugate Margins Conference 2010*, **5**, 216-219.

Pérez-Gussinyé, M. & Reston, T. J. 2001. Rheological evolution during extension at nonvolcanic rifted margins: onset of serpentinization and development of detachments leading to continental breakup. *Journal of Geophysical Research - Solid Earth*, **106**(B3), 3961-3975, doi:10.1029/2000JB900325.

Readman, P. W., O’Reilly, B. M., Shannon, P. M. & Naylor, D. 2005. The deep structure of the Porcupine Basin, offshore Ireland, from gravity and magnetic studies. In *Geological Society, London, Petroleum Geology Conference series*, **6**, 1047-1056, doi:10.1144/0061047.

Reston, T. J., Pennell, J., Stubenrauch, A., Walker, I. & Pérez-Gussinyé, M. 2001. Detachment faulting, mantle serpentinization, and serpentinite-mud volcanism beneath the Porcupine Basin, southwest of Ireland. *Geology*, **29**(7), 587-590, doi:10.1130/0091-7613(2001) 029<0587:DFMSAS>2.0.CO;2.

Reston, T. J., Gaw, V., Pennell, J., Klaeschen, D., Stubenrauch, A. & Walker, I. 2004. Extreme crustal thinning in the south Porcupine Basin and the nature of the Porcupine Median High:

implications for the formation of non-volcanic rifted margins. *Journal of the Geological Society*, **161**(5), 783-798, doi:10.1144/0016-764903-036.

Ryan, W.B., Carbotte, S.M., Coplan, J.O., O'Hara, S., Melkonian, A., Arko, R., Weissel, R.A., Ferrini, V., Goodwillie, A., Nitsche, F. & Bonczkowski, J. 2009. Global multi-resolution topography synthesis. *Geochemistry, Geophysics, Geosystems*, **10**(3), doi:10.1029/2008GC002332.

Sallarès, V., Gailler, A., Gutscher, M. A., Graindorge, D., Bartolomé, R., Gracia, E., Díaz, J., Dañobeitia, J.J. & Zitellini, N. 2011. Seismic evidence for the presence of Jurassic oceanic crust in the central Gulf of Cadiz (SW Iberian margin). *Earth and Planetary Science Letter*, **311**(1), 112-123, doi:10.1016/j.epsl.2011.09.003.

Shannon, P. M. 1991. The development of Irish offshore sedimentary basins. *Journal of the Geological Society*, **148**(1), 181-189, doi:10.1144/gsjgs.148.1.0181.

Stockwell, J. W. 1999. The CWP/SU: Seismic Un*x package. *Computers & Geosciences*, **25**, 415-419, doi:10.1016/S0098-3004(98)00145-9.

Tate, M. P., White, N. & Conroy, J.-J. 1993. Lithospheric extension and magmatism in the Porcupine Basin west of Ireland. *Journal of Geophysical Research - Solid Earth*, **98**, 13 905-13 923, doi:10.1029/93JB00890.

Tate, M. P. & Dobson, M. R. 1988. Syn-and post-rift igneous activity in the Porcupine Seabight Basin and adjacent continental margin W of Ireland. *Geological Society, London, Special Publications*, **39**(1), 309-334, doi:10.1144/GSL.SP.1988.039.01.28.

Wangen, M. 2010. *Physical principles of sedimentary basin analysis*. Cambridge University Press.

Welford, J.K., Shannon, P.M., O'Reilly, B.M. and Hall, J. 2012. Comparison of lithosphere structure across the Orphan Basin–Flemish Cap and Irish Atlantic conjugate continental margins from constrained 3D gravity inversions. *Journal of the Geological Society*, **169**(4), 405-420, doi:10.1144/0016-76492011-114.

Wessel, P. & Smith, W. H. 1998. New, improved version of Generic Mapping Tools released. *Eos, Transactions American Geophysical Union*, **79**, 579-579, doi:10.1029/98EO00426.

White, N., Tate, M. & Conroy, J. J. 1992. Lithospheric stretching in the Porcupine Basin, west of Ireland. *Geological Society, London, Special Publications*, **62**(1), 327-331, doi:10.1144/GSL.SP.1992.062.01.25.

White, N., Thompson, M. & Barwise, T. 2003. Understanding the thermal evolution of deep-water continental margins. *Nature*, **426**, 334-343, doi:10.1038/nature02133.

Wrigley, R., Intawong, A. & Rodriguez, K. 2014. Ireland Atlantic Margin: a new era in a frontier basin. *First Break*, **32**(12), 95-100.

Zelt, C. A., & Forsyth, D. A. 1994. Modeling wide-angle seismic data for crustal structure: Southeastern Grenville Province. *Journal of Geophysical Research - Solid Earth*, **99**, 11687-11704, doi:10.1029/93JB02764.

TABLES

Table 1. *Modelling statistics for the northern line*. The “refr” (refractions) and “refl” (reflections) subscripts refer to the parts of dataset considered.

Step	Iteration*	N_{refr}†	N_{refl}†	$t_{RMS\text{-}refr}$‡	$t_{RMS\text{-}refl}$‡	$t_{RMS\text{-}all}$‡	χ^2_{refr}§	χ^2_{refl}§	χ^2_{all}§
1	4	654	1,050	32	31	32	1.18	0.22	0.58
2	9	978	886	25	32	28	0.82	0.13	0.49
3	9	2,399	3,445	20	38	32	0.48	0.25	0.35
4	9	4,410	4,124	17	29	23	0.29	0.12	0.21
5	9	5,955	1,819	36	83	51	0.98	1.04	0.99
6	4	15,580	3,004	58	95	65	0.60	1.11	0.69
7	4	17,348	3,004	61	84	65	0.62	0.91	0.66

*Iteration chosen to build the input model of next step (or final model for step 7).

†Numbers of picks used for the modelling.

‡Root mean squared travel-time residuals, in milliseconds.

§Normalised chi-squared.

Table 2. *Modelling statistics for the southern line*. The “refr” (refractions) and “refl” (reflections) subscripts refer to the parts of dataset considered.

Step	Iteration*	N_{refr}†	N_{refl}†	$t_{RMS\text{-}refr}$‡	$t_{RMS\text{-}refl}$‡	$t_{RMS\text{-}all}$‡	χ^2_{refr}§	χ^2_{refl}§	χ^2_{all}§
1	4	1,952	2,149	15	30	24	0.56	0.59	0.58
2	3	4,685	5,491	19	27	24	0.44	0.29	0.36
3	5	8,163	3,638	38	58	45	0.51	0.67	0.56
4	4	15,502	8,563	47	70	56	0.48	0.89	0.63
5	4	23,520	13,209	54	86	67	0.43	0.87	0.59
6	2	29,927	13,209	69	84	74	0.59	0.84	0.67

*Iteration chosen to build the input model of next step (or final model for step 6).

†Numbers of picks used for the modelling.

‡Root mean squared travel-time residuals, in milliseconds.

§Normalised chi-squared.

FIGURE CAPTIONS

Fig. 1. Location map.

(**a**) Location of the study area relative to Western Europe. (**b**) Bathymetric map of the study area showing location of the two refraction profiles presented. Black lines show the location of the shots along the northern and southern profiles. Bathymetry and elevation data are from Ryan *et al.* (2009). Yellow circles show the positions of the ocean bottom instruments, which recorded the data used for the seismic refraction processing. Grey circles are the instruments that failed to record usable data. The coloured lines and the grey zone in the centre of the basin correspond to the values of stretching factors estimated from subsidence analysis and the location of the Porcupine Median Ridge (PMR), respectively, from Tate *et al.* (1993). The red box shows the location of the map in part (c). The red stars show the location of the wells presented in Fig. 5. (**c**) Detailed gravity map around the two profiles presented in this study. Colour and symbol codes are the same as for part (b). Black numbers refer to the instrument numbers.

Fig. 2. Examples of data and phase picking.

Data were deconvolved and filtered for display. Colour bars represent the picks; colour codes are detailed at the bottom of the figure. The height of each pick corresponds to its uncertainty. Every sixth pick is shown. Black arrows show arrivals from a high-velocity layer that we chose to ignore for the tomography modelling. (**a**) OBS 51, vertical geophone, along the northern line. (**b**) Same as (a) with picks. (**c**) OBS 60, vertical geophone, along the northern line. (**d**) Same as (c) with picks. (**e**) OBH 20 along the southern line. (**f**) Same as (e) with picks. (**g**) OBH 93 along the southern line. (**h**) Same as (g) with picks. Different reduction velocities were used for each plot; these are specified in the label of the reduced time axis.

Fig. 3. Velocity models and derivative weight sums for the two profiles.

(**a**) Velocity model obtained after layer-stripping tomography modelling along the northern line. Coloured interfaces show the interfaces used for the layered modelling, where they are illuminated by wide-angle reflections. Colour codes are detailed in the lower right corner of the figure. Numbers above instruments indicate the location of the instruments shown in Fig. 2. (**b**) Velocity model for the southern profile. Colour codes are the same as for part (a) of this figure. (**c**) Derivative Weight Sum (DWS) for the northern profile. High DWS indicates regions with dense ray coverage, i.e. regions with the best velocity resolution. (**d**) DWS for the southern profile.

Fig. 4. Selection of vertical velocity profiles.

(**a**) Northern line. (**b**) Southern line.

Fig. 5. Comparisons between P-wave velocities and nearby sonic logs from wells calibrated by check-shot data.

Borehole velocities were digitised from analogue records. (**a**) Northern line. (**b**) Southern line. No data were acquired in the first 600 m. below seafloor.

Fig. 6. Comparison between velocity model of the Northern profile and coincident seismic reflection data.

(**a**) Time migrated section of Wire 2 profile (Croker & Klemperer 1989). (**b**) Pre-stack depth migrated section of Wire 2. Red arrows highlight deep reflectors, interpreted as Moho reflections. Numbers above instruments indicate the location of the instruments shown in Fig. 2. (**c**) Superposition of the results for the Northern profile on Wire 2.

Fig. 7. Comparison between velocity model of the Southern profile and coincident seismic reflection data.

(**a**) Time migrated section of SPB97-115. (**b**) Pre-stack depth migrated section of SPB97-115. Blue arrows indicate a highly reflective layer, interpreted as igneous. Red arrows highlight deep reflectors, interpreted as Moho reflections. Numbers above instruments indicate the location of the instruments shown in Fig. 2. (**c**) Superposition of the results for the Southern profile on SPB97-115.

Figure 1

Click here to download Figure Trackmap_fig1.png

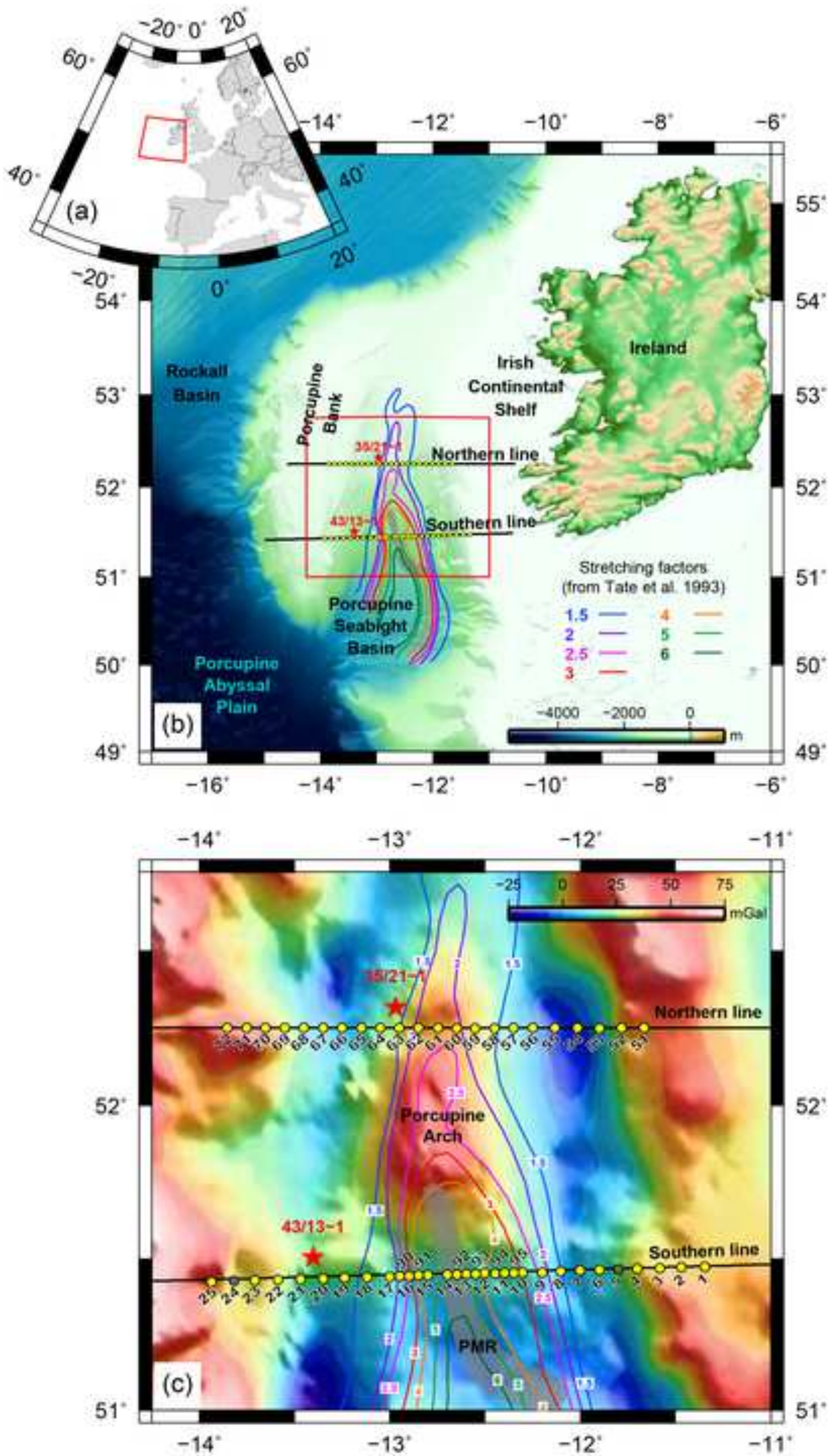

Figure 2

Click here to download Figure Sismos_Picks_fig2.png

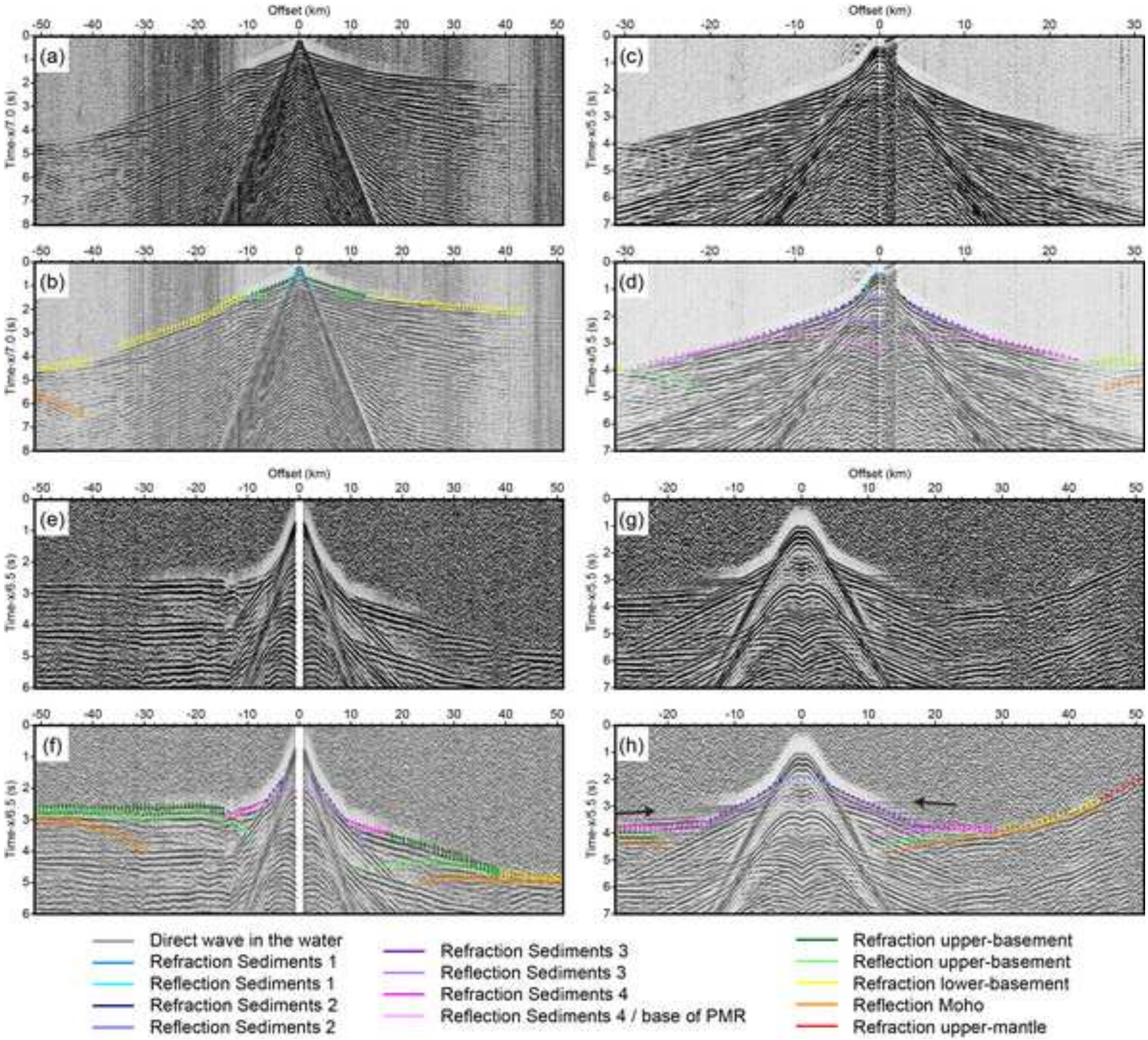

Figure 3

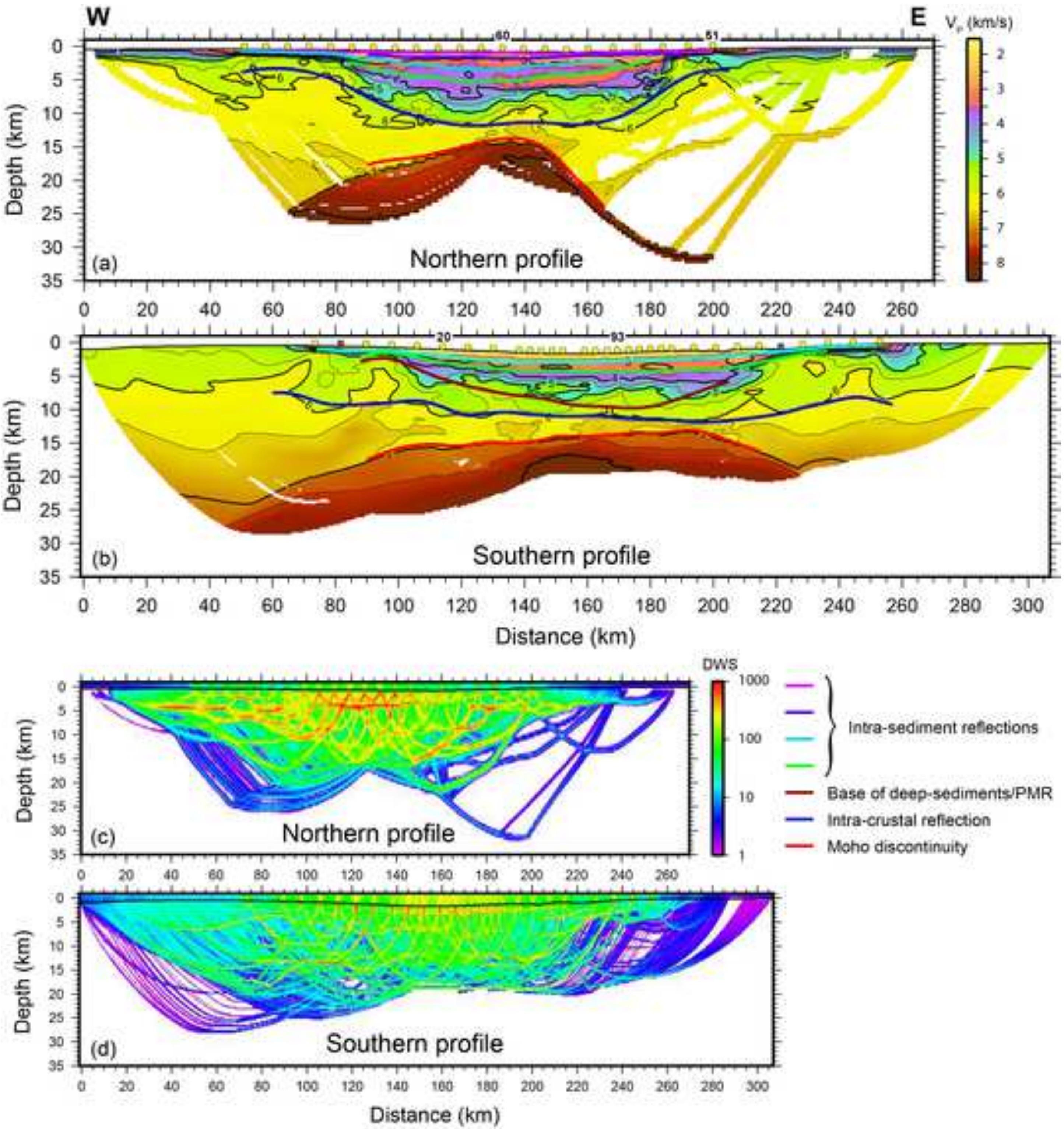
W
E
V_p (km/s)
Depth (km)
(a)
Northern profile
(b)
Southern profile
Distance (km)
DWS
(c)
Northern profile
(d)
Southern profile
Intra-sediment reflections
Base of deep-sediments/PMR
Intra-crustal reflection
Moho discontinuity

Figure 4

Click here to download Figure V1D_fig4.png

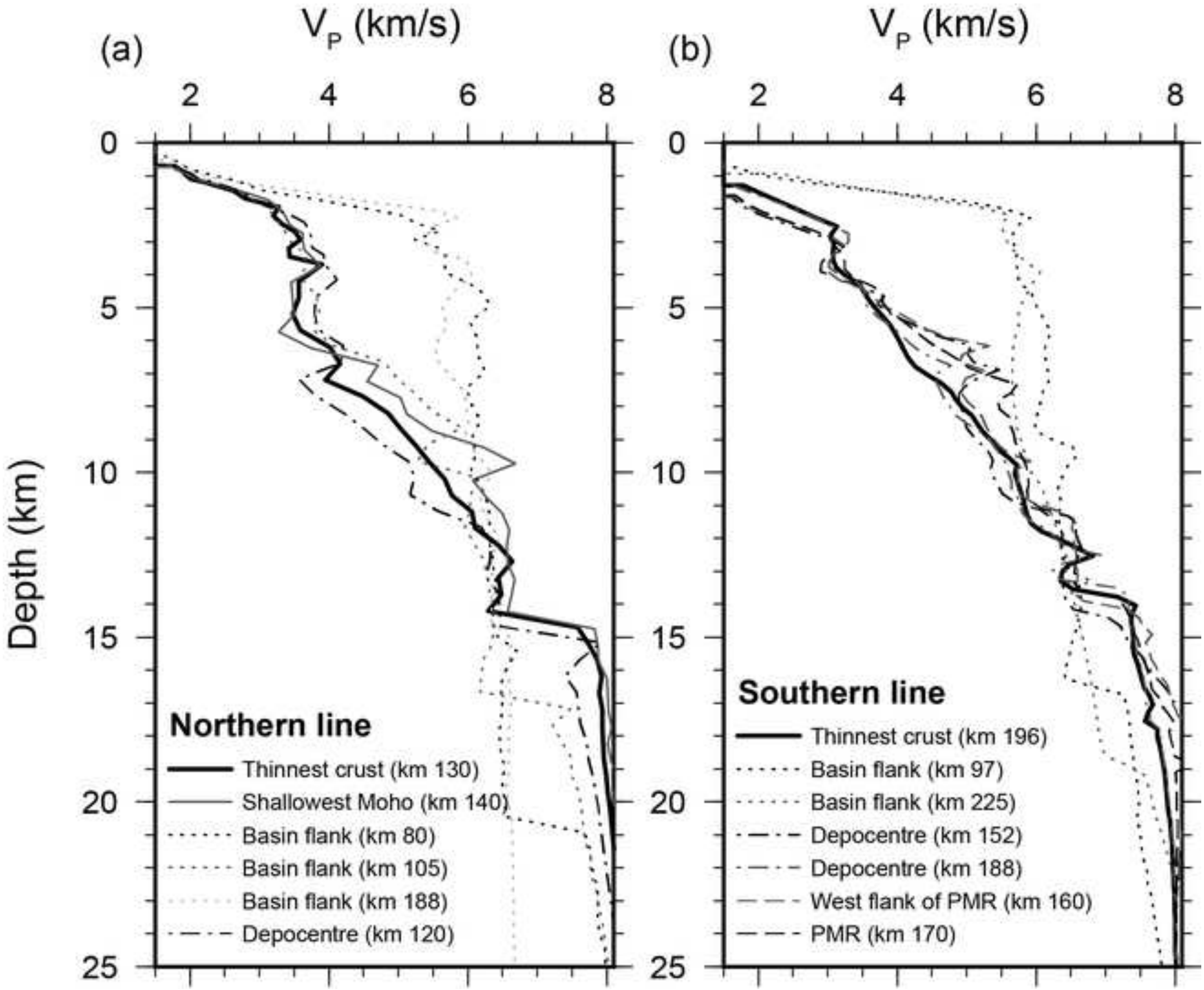

Figure 5

Click here to download Figure Wells_fig5.png

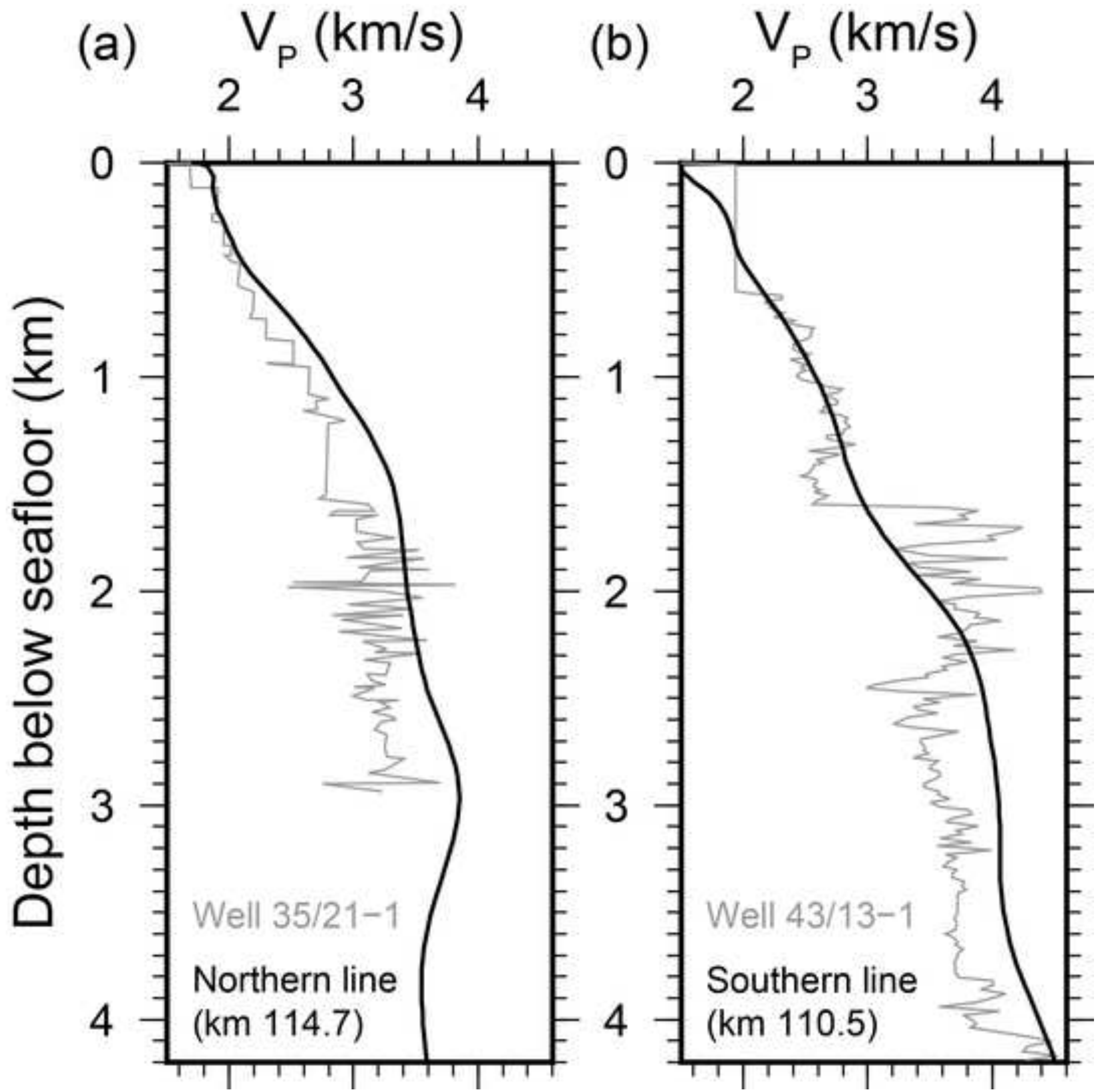

Figure 6

Click here to download Figure Overlay_MCS_North_fig6.png

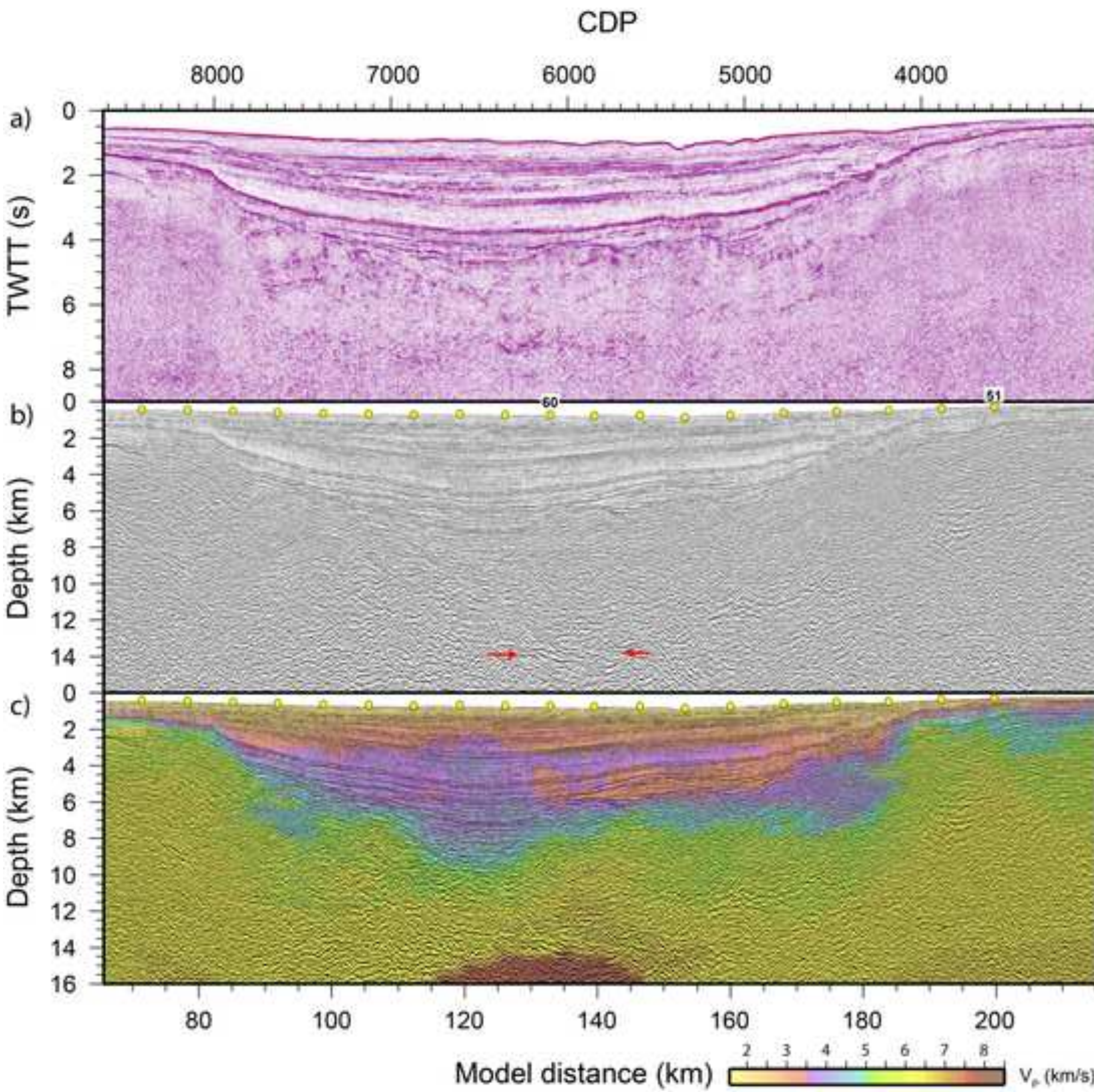

Figure 7

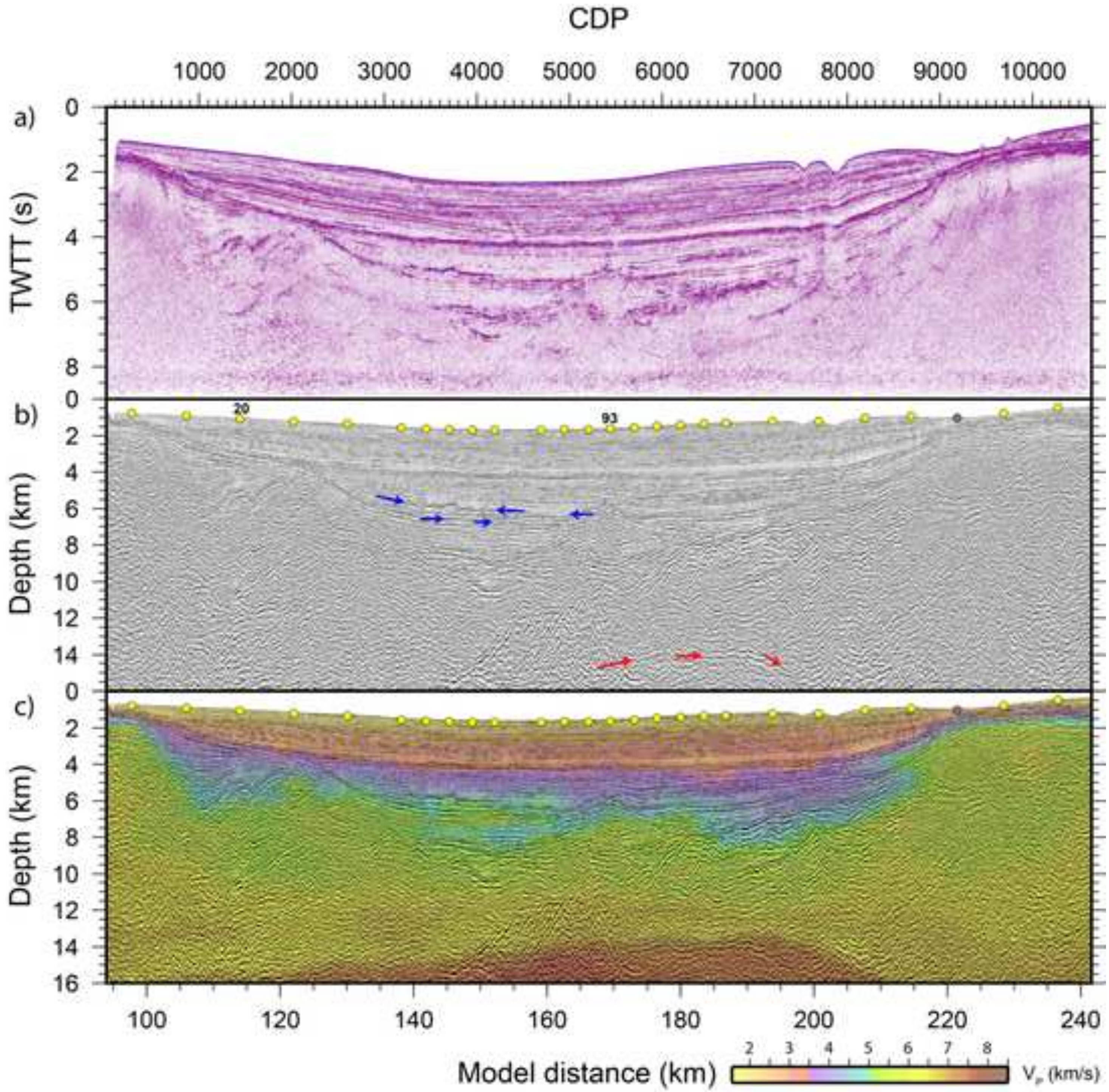
CDP
1000
2000
3000
4000
5000
6000
7000
8000
9000
10000
a)
TWTT (s)
0
2
4
6
8
b)
Depth (km)
20
93
c)
Depth (km)
0
2
4
6
8
10
12
14
16
100
120
140
160
180
200
220
240
Model distance (km)
2 3 4 5 6 7 8
V_p (km/s)